RSC Advances

PAPER

View Article Online
View Journal | View Issue

Cite this: *RSC Adv.*, 2025, **15**, 41314

Electrochemical detection of chlorogenic acid in green coffee beans by a carbon paste electrode modified with MWCNTs and Cr-MOF

Maryam Khayatkashani,[a] Safaa Abdulkadhim Almansarawi,[b] Ebrahim Honarmand,*[c] Fateme Sadat Sadeghi,[a] Ali Ehsani,[a] Layth S. Jasim[d] and Masoud Salavati-Niasari*[e]

The purpose of this study is to address the need for rapid and selective detection of chlorogenic acid (CGA), a bioactive polyphenol with considerable medicinal importance. There are various techniques to determine the amount of CGA, but electrochemical methods are a cost-effective and efficient alternative. In this study, an efficient electrochemical sensor was prepared for the detection and measurement of CGA in green coffee samples. A composite of MIL-101(Cr) and MWCNTs was utilized to modify the carbon paste electrode (CPE). The metal–organic framework (MOF) was used due to its high surface area and known catalytic activity. The modified sensor showed improved electron-transfer and absorption capabilities, leading to a low detection limit and a wide linear range. The structure of the Cr-MOF and MWCNT compounds synthesized in this work was determined and analyzed using FT-IR, EDX, SEM, and XRD techniques. Electrochemical impedance spectroscopy (EIS) and cyclic voltammetry (CV) were also used to investigate the electrochemical efficiency of the modified electrode. Under optimal conditions, the differential pulse voltammetry (DPV) diagram showed that the relationship between the CGA concentration and current intensity is in two linear ranges, with a determination coefficient of 0.9855 in concentrations from 0 to 14.4 μM and a determination coefficient of 0.9962 in concentrations from 14 to 177.6 μM. The limit of detection (LOD) was 0.0198 μM. Finally, the modified sensor was validated using a standard UV-vis method.

Received 18th July 2025
Accepted 26th September 2025

DOI: 10.1039/d5ra05186j

rsc.li/rsc-advances

1. Introduction

Polyphenolics are a group of natural compounds found in some plants and fruits, which have recently received attention due to their antioxidant properties.[1] These compounds consist of quinic acid and various dihydroxycinnamic acids, including ferulic acid, caffeic acid, *p*-coumaric acid and chlorogenic acid.[2–5] Chlorogenic acid (CGA) is found in many products, including beverages, such as coffee and green tea; fruits, like apples, peaches, apricots and strawberries; vegetables, such as tomatoes, carrots and eggplants; and hundreds of medicinal plants, including honeysuckle, *Eucommia ulmoides*, and *Calendula officinalis*.[6–9] The CGA present in plants has a protective effect against pathogenic and destructive agents. CGA also prevents the enzymatic color change of vegetables and fruits.[10] In recent years, many clinical studies have been conducted on the various aspects of human health associated with the regular consumption of foods containing chlorogenic acid.[11] The results of these studies show the medicinal role of CGA on human physiological activities, including its antioxidant, antimicrobial, antiviral, antibacterial, anti-stress, anti-inflammatory and anti-cancer properties.[5,8,12–15] CGA also has a major effect in protecting the liver and is one of the effective factors in controlling glucose metabolism and reducing its level in the blood, which is very useful for treating diabetes.[16,17] On the other hand, the concentration of CGA in the human body should be controlled because high concentrations of CGA lead to some disorders and inflammatory reactions, including nausea and diarrhea, high stress and the occurrence of dermatitis, itching and eczema.[5,18–20] Therefore, the quantitative measurement of CGA has received much attention. Many methods have been developed to measure CGA in coffee plants and beans, such as high-performance liquid chromatography,[21,22] capillary electrophoresis,[23,24] micellar electrokinetic chromatography,[25] liquid chromatography-mass spectrometry,[26] near-infrared spectroscopy,[27] and electrochemical

[a]*Advanced Medical Pharma (AMP-Biotec), Biopharmaceutical Innovation Centre, Via Cortenocera, 82030, San Salvatore Telesino, BN, Italy*

[b]*Department of Chemistry, University of Sumer, College of Education, Thi-Qar, Iraq*

[c]*Department of Chemistry, Faculty of Science, University of Qom, Qom, Iran. E-mail: e.honarmand@qom.ac.ir*

[d]*Department of Chemistry, College of Education, University of Al-Qadisiyah, Diwaniyah, Iraq*

[e]*Institute of Nano Science and Nano Technology, University of Kashan, P.O. Box 87317-51167, Kashan, Iran. E-mail: salavati@kashanu.ac.ir; Fax: +98 31 55913201; Tel: +98 31 55912383*

methods.[28,29] Although these methods are efficient for measuring CGA, a number of deficiencies were identified, mainly their long and time-consuming steps and the need for expensive instruments for their implementation. To resolve the challenges caused by these deficiencies, electrochemical methods have been widely investigated in recent years due to their low cost, simplicity, fast response and high sensitivity for the detection of various compounds. However, most electrocatalysts have disadvantages related to their low active surface area and low density of active sites. Therefore, the development of sensing materials is very important for improving the electrochemical performance of electrocatalysts.[30]

Beyyavaş *et al.* reported a method in which a glassy carbon electrode (GCE) was modified with CNTs alongside gadolinium oxide and tungsten nanoparticles for the sensitive determination of CGA. This method achieved a linear range of 2.5×10^{-9}–1.6×10^{-6} M with a detection limit of 1.08×10^{-9} M.[31] Wan *et al.* synthesized Fe_3O_4/SiO_2/PIL, which has good magnetic properties, a suitable structure and high stability, for detecting the CGA concentration in fruit samples and it showed a linear relationship in the concentration range of 0.025–2 mM ($R^2 = 0.9989$) with a detection limit of 10 nM.[32] In another study, a composite iron oxide/zinc oxide (Fe_3O_4/ZnO) modified-GCE based on a binary metal oxide was used for the determination of CGA. The electrochemical evaluation of CGA by Fe_3O_4/ZnO/GCE showed a relatively wide linear range between 0.05–1291 μM using LSV. Additionally, the detection sensitivity of the sensor was 0.05 μA μM^{-1} cm^{-1-2}.[33] Mariyappan *et al.* reported the use of Co-MOF/BP-RGO on a GCE with a high selectivity for the detection of CGA that showed a wide linear range and an excellent LOD of 0.001–391 μM and 0.014 μM, respectively.[5] Amalraj *et al.* reported a GCE modified with Bi_2CuO_4–KOH for the electrochemical measurement of CGA, having a linear range of 0.05–556 μM and a sensitivity of 0.22 μA μM^{-1} cm^{-1-2}.[34] Teker *et al.* reported a novel voltammetric method for the high-sensitivity measurement of CGA using a glassy carbon electrode modified with niobium nanoparticles (NbNPs) and MWCNTs.[29]

CGA is a polyphenolic compound with multiple hydroxyl groups and aromatic rings, requiring a sensor with high surface area, selective adsorption, and efficient electron transfer. Metal–organic frameworks (MOFs) possess tunable porosity, abundant active sites, and large surface area, enabling strong interactions with CGA *via* hydrogen bonding and π–π stacking.[35] MOFs are crystalline materials that have a highly ordered network structure.[36] Due to their remarkable properties, including structural flexibility, adjustable pores, high storage capacities,[37] and suitable thermal and chemical stability, they are widely used in applications such as gas storage and separation,[38] as catalysts[39] and as delivery systems.[40] In this study, MIL-101(Cr) was chosen because of its extremely high surface area and large pore volume, which enhance the adsorption and accessibility of CGA, and its unsaturated Cr(III) sites, which promote efficient electron transfer during CGA oxidation. In addition, the appropriate chemical stability of this framework and its ability to interact with phenolic molecules through strong hydrogen bonding and π–π stacking interactions indicate its high sensitivity and selectivity for the electrochemical detection of CGA.[41] The use of MOFs as modulators for electrochemical sensors has increased in recent years due to their high catalytic activity, suitable chemical performance and adjustable pores, as well as the metal centers in their structure that facilitate the oxidation of analytes on their surface.[42,43] Nevertheless, some of their characteristics, such as the limited mass transfer of analytes and low electrical conductivity, limit their further use.[44] One approach for addressing these limitations is combining metal–organic frameworks (MOFs) with materials that have a high electrical conductivity to create composites based on these structures. One example is carbon-based materials, which are a good choice due to their good electrochemical stability and high conductivity. These carbon-based materials include graphene oxide,[45] carbon nanotubes (CNTs)[46] and carbon nanofibers.[47]

Carbon nanotubes are a type of graphite sheet that exist in a tubular form with nanometer-sized diameters. If one graphite sheet is in a tubular form, it is called a single-walled carbon nanotube; if several graphite sheets are in a tubular form, they are called multi-walled carbon nanotubes.[48] There is a very high potential for the use of CNTs in science and technology applications to improve the electrical and thermal conductivity properties. Other CNT applications include medical and dye industries, corrosion protection, electromagnetic interference protection, batteries, solar cells, and chemical sensing.[49–51] Due to the high conductivity of carbon nanotubes and their enhanced electron-transfer kinetics, these materials can be used in electrodes. Electrodes based on CNTs afford increased sensitivity and ability to detect and measure species at low concentrations.[52]

In this study, an electrochemical sensor based on a metal–organic compound was designed to measure CGA. Therefore, MIL-101(Cr) was synthesized and then combined with carbon nanotubes whose surface was modified to increase the conductivity of the carbon paste electrode. The results of this study show the benefit derived from the high conductivity of carbon nanotubes along with their high surface absorption capability for measurements. Finally, a high-sensitivity electrode for measuring CGA in coffee samples is presented, which is selective, sensitive and displays good reproducibility.

2. Experimental

2.1. Reagents and chemicals

Potassium hydroxide, chlorogenic acid ($C_{16}H_{18}O_9$, 98%), multi-walled carbon nanotubes (MWCNTs, >97%), ethanol (96%), and 0.1 M phosphate buffer solution (PBS) were used for the preparation of solutions (Na_2HPO_4 and NaH_2PO_4). Potassium ferricyanide ($K_3[Fe(CN)_6]$), potassium ferrocyanide ($K_4[Fe(CN)_6]$), chromium nitrate nonahydrate ($Cr(NO_3)_3 \cdot 9H_2O$), benzene dicarboxylic acid (BDC), ammonium fluoride (NH_4F), dimethylformamide (DMF), and green coffee beans were also used in this study.

2.2. Characterization

In order to perform electrochemical tests, a potentiostat/galvanostat device (Ivium V21508, Vertex) with a three-

electrode system comprising a Ag/AgCl reference electrode in a saturated solution of KCl, platinum rod counter electrode (Azar Electrode Company) and a carbon paste working electrode was used. The morphology and characteristics of the prepared composites were studied using SEM images along with EDX analysis, FTIR spectroscopy and XRD analysis.

2.3. Functionalization of MWCNTs

In order to functionalize the carbon nanotubes, 0.6 g of the multi-walled carbon nanotube sample was placed with 100 ml of the acidic mixture comprising 26.0 ml of sulfuric acid and 74 ml of nitric acid [1 : 3] in a water-bath at a temperature of 85 °C for 3 hours. After centrifuging and washing eight times with deionized water, the obtained product was placed in an oven at a temperature of 80 °C and dried for 12 hours.[53]

2.4. Synthesis of MIL-101(Cr)

To synthesize MIL-101(Cr), 6.0 g of $Cr(NO_3)_3 \cdot 9H_2O$, 2.5 g of BDC, and 71.0 ml of deionized water were placed into a 150.0-ml Teflon container. This container was then heated in a stainless-steel autoclave at 220 °C for 8 hours. Following heating, the mixture was gradually cooled to room temperature over a period of 4 hours. The resulting MIL-101(Cr) was initially washed with deionized water. To achieve an enhanced purity, the product was subsequently washed with an aqueous solution of 80% ethanol. After centrifugation, the dried, green powder was then weighed and based on a ratio of 1.0 g in 150.0 ml, it was stirred in an aqueous solution of 30 mM NH_4F at 60 °C for 10 hours. The suspension was centrifuged and washed with warm deionized water. Subsequently, the green solid was washed with 100.0 ml of DMF and then washed with 120.0 ml of deionized water. Finally, the product was dried for two days at room temperature, followed by an additional two days in an oven set at 95 °C.[54]

2.5. Manufacturing the modified electrode

In this study, four types of carbon paste electrodes were prepared. The initial carbon paste was composed of 0.15 g of graphite powder and 0.03 g of pure liquid paraffin oil, maintaining a weight ratio of 20 : 80. These components were thoroughly mixed in a mortar for 10 min. To modify the carbon paste with a metal–organic framework (MOF), 10 wt% of the graphite powder was replaced with MIL-101(Cr), which was dissolved in 2 ml of ethanol and subjected to an ultrasonic treatment for 10 min. After the mixture was homogenized and dried in an oven, it was combined with paraffin oil in a weight ratio of 70 : 10 : 20. The carbon paste modified with carbon nanotubes (CNTs) was prepared using a similar method. The electrodes modified with both MOF and CNTs were obtained by replacing equal amounts of multi-walled carbon nanotubes (MWCNTs) and MOF in the graphite powder and paraffin oil, resulting in a weight ratio of 60 : 10 : 10 : 20. The prepared pastes were loaded into insulin syringes, and their surfaces were smoothed using weighing paper. Electrical connections were established using copper wire. To ensure optimal performance, the surfaces of the electrodes were polished and refreshed after each experimental run.

3. Results and discussion

3.1. Characterization

3.1.1. SEM and EDX mapping analyses. FE-SEM analysis was performed to investigate the surface morphology of Cr-MOF, MWCNTs, and Cr-MOF-MWCNTs/CPE. Fig. 1(a and b) shows the FE-SEM images of Cr-MOF. These images reveal that the synthesized framework had polyhedral crystalline forms (octahedral crystals of the MIL-101(Cr) network), which agree with previous reports.[54] In addition, the absence of needle-shaped crystals—indicative of unreacted H2BDC ligand—in the powder suggests that the synthesis was a well-optimized and complementary process. Moreover, based on the image size, particles and crystals are visible in the figure, revealing that the synthesized MIL-101(Cr) exhibits a size of less than 200 nm. Fig. 1(c and d) presents the FE-SEM images of the MWCNTs. The FE-SEM images reveal nanosized, multi-walled carbon nanotubes whose surfaces were activated by the combination of sulfuric acid and nitric acid. Fig. 1(e and f) depicts the FE-SEM images of the electrode paste made from the combination of graphite, MOF and MWCNTs and further reveals the uniformity of the paste that resulted from the combination of these materials. MWCNTs are distributed around the MIL-101(Cr) framework, resulting from molecular interactions between the –COOH groups and Cr^{3+} ions present in the metal–organic structure. Fig. 1(g–i) shows the percentage of elements in each composition. The percentage of carbon and oxygen in the MWCNTs is higher than their percentage in the combination of MWCNTs and MIL101-(Cr). This observation is attributable to the composition of the carbon paste, where a percentage of its total composition is related to the chromium element. Additionally, the percentage of chromium element in MIL101-(Cr) is higher than its percentage in the carbon paste; aside from the abovementioned elements, no additional elements were found in the elemental analysis. The EDX mapping images of the carbon paste modified with MIL-101(Cr) and MWCNTs are presented in Fig. 1(j). Each element in the figure is shown with a specific color (blue, red, and green). In the carbon paste composition, the dispersion of colors (particles) can be well observed, indicating the uniformity of the modifiers in the carbon paste.

3.1.2. XRD analysis. The X-ray diffraction (XRD) data for the MWCNTs and MIL-101(Cr) are shown in Fig. 2(a) and (b), respectively. In Fig. 2(a), the XRD pattern of the modified multi-walled carbon nanotubes is shown, which was recorded at an angle of 2θ equal to 4 to 80°. The diffraction peaks observed at 26° and 44° are related to the (0 0 2) and (1 0 0) reflections, respectively, which are related to the hexagonal graphite present in the carbon nanotubes. The XRD pattern for the synthesized MIL-101(Cr) sample in this study is displayed over the 2θ range from 4° to 60°. The XRD results reveal distinct peaks at angles of 8.5°, 9.2°, 17°, 27°, and 35°. A comparative assessment with standard patterns found in the literature indicates that these

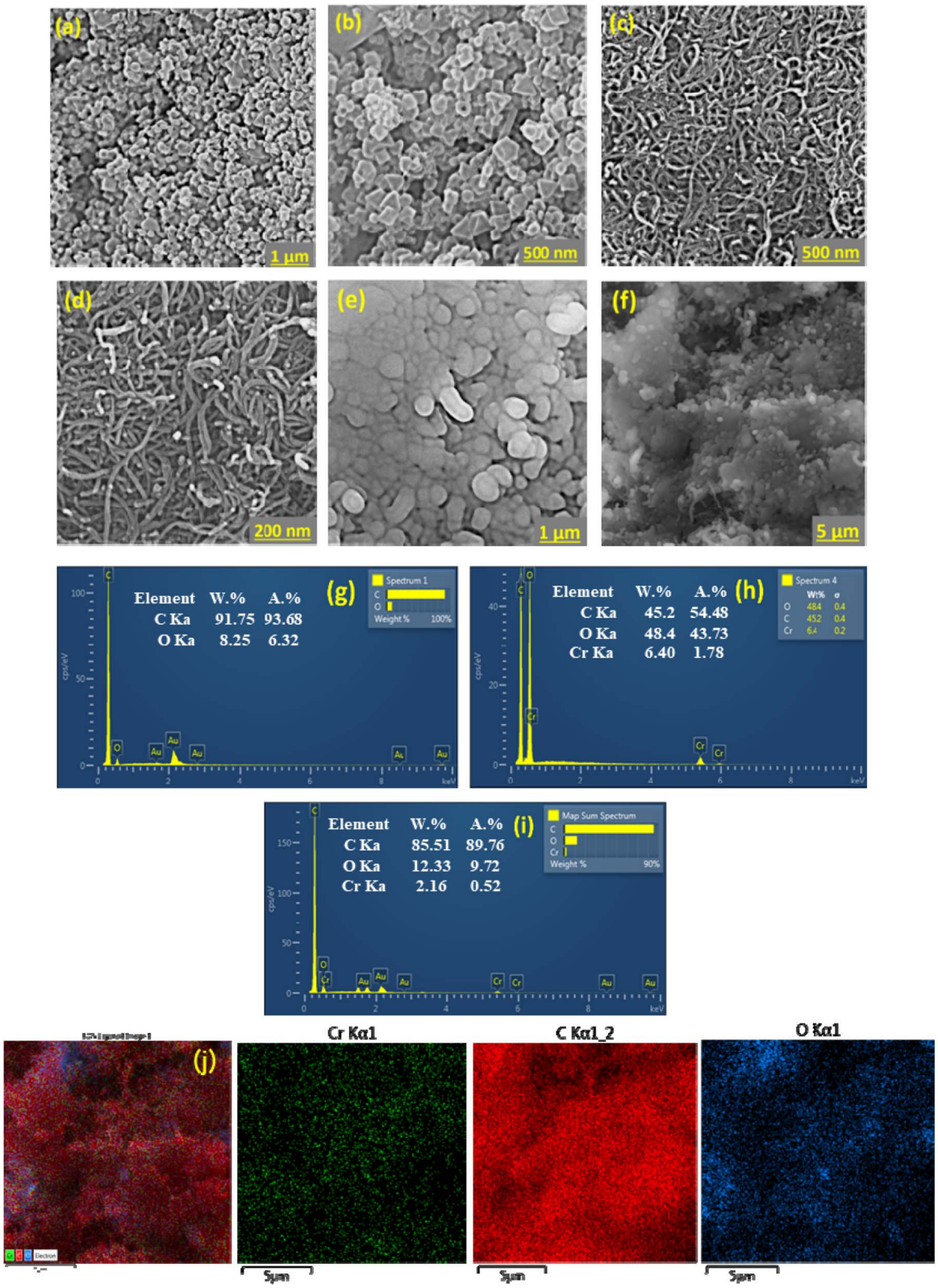

Fig. 1 FE-SEM images of (a and b) Cr-MOF, (c and d) MWCNTs and (e and f) Cr-MOF-MWCNTs/CPE. EDS spectra of (g) MWCNTs, (h) Cr-MOF and (i) Cr-MOF-MWCNTs/CPE. (j) EDS mapping images of Cr-MOF-MWCNTs/CPE.

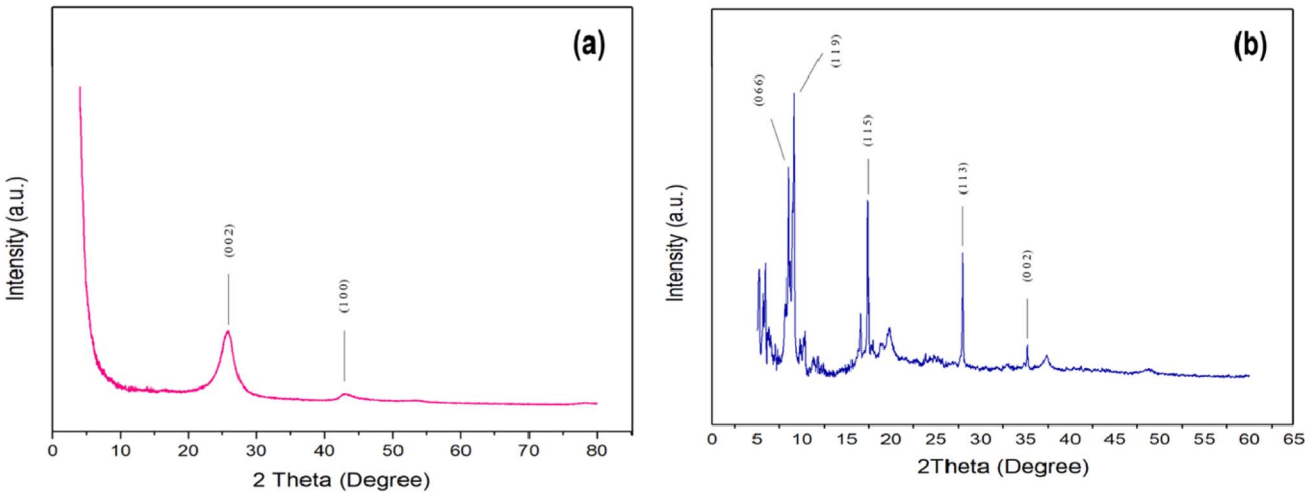

Fig. 2 XRD patterns of (a) MWCNTs and (b) MIL-101(Cr).

peaks correspond to the (0 6 6), (1 1 9), (1 1 5), (1 1 3), and (0 0 2) crystalline planes, respectively.[55]

3.1.3. FT-IR characterization. Fig. 3(a and b) shows the FT-IR spectra of the MWCNTs and MIL-101(Cr). The FT-IR spectrum in Fig. 3(a) is related to the structure of the acid-modified MWCNTs. The peak in the wavenumber range of 3200–3600 cm^{-1} is related to OH groups, and the absorption peak of the stretching vibration of the –C═O– bond appears in the range of 1755–1670 cm^{-1}; in particular, the peaks at 1552 and 1710 cm^{-1} are related to this bond.[56] In the FT-IR spectrum shown in Fig. 3(b), the peaks in the wavenumber range of 4000–500 cm^{-1} correspond to the structure of the synthesized MIL-101(Cr). The 1400 cm^{-1} and 1609 cm^{-1} bands were assigned to the symmetric stretching vibration of the O–C–O bond in MIL-101(Cr). The other bands between 600 cm^{-1} and 1600 cm^{-1} confirmed the presence of a benzene ring; these peaks include the C═C stretching vibration at 1505 cm^{-1} and C–H bond deformation vibrations at 747 cm^{-1} and 1018 cm^{-1}. The peaks related to the stretching vibrations of oxygen with metals, which are usually observed in the range of 400–800 cm^{-1}, are also observed in this spectrum. The peak at 508 cm^{-1} corresponds to the Cr–O bond vibration.[57,58]

3.1.4. Electrochemical characterization of Cr-MOF-MWCNTs/CPE. Cyclic voltammetry (CV) was used to investigate the effects of different modifiers on the carbon paste electrode. Fig. 4(a) shows the cyclic voltammograms (CVs) of the different modified CPEs: MWCNTs/CPE, Cr-MOF/CPE and Cr-MOF-MWCNTs/CPE electrodes in 0.1 M KCl solution containing 5 mM $[Fe(CN)_6]^{3-/4-}$. The iron tracer solution showed two oxidation and reduction peaks for all four electrodes. The

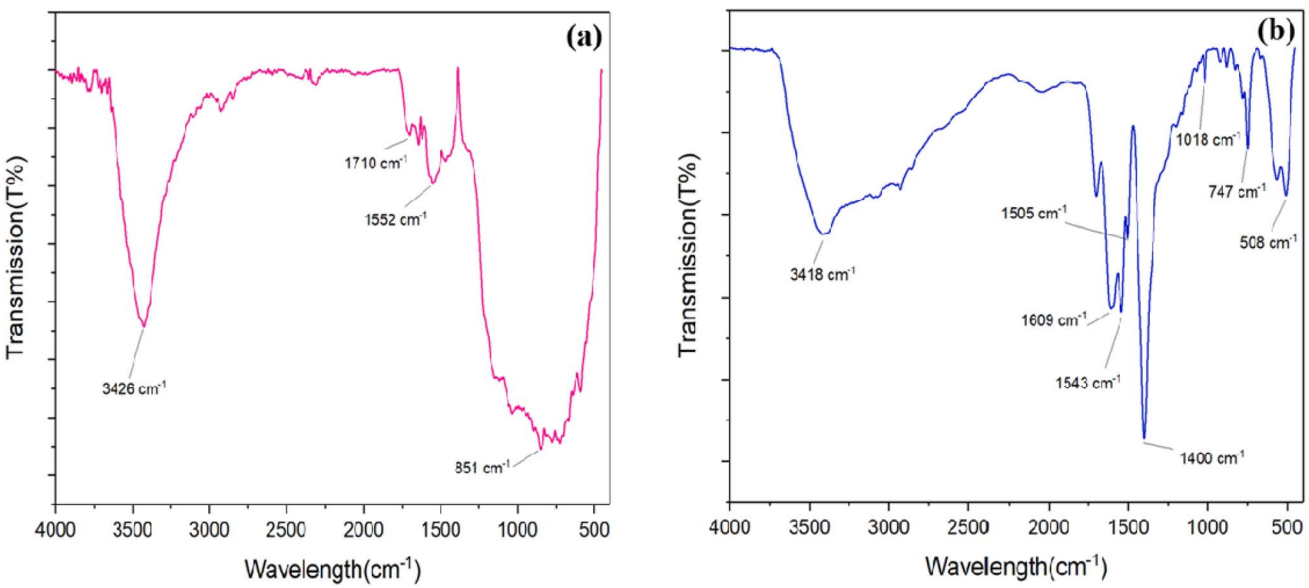

Fig. 3 FT-IR spectra of (a) MWCNTs and (b) MIL-101(Cr).

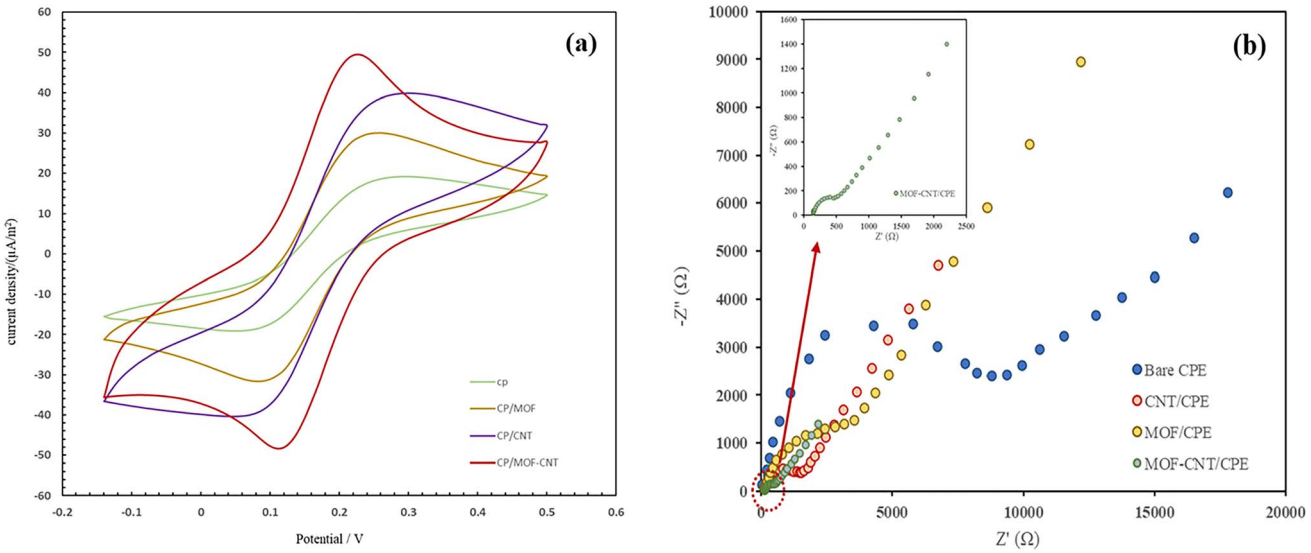

Fig. 4 (a) Cyclic voltammograms and (b) Nyquist diagrams of different modified electrodes, CPE, MWCNTs/CPE, Cr-MOF/CPE, and Cr-MOF-MWCNTs/CPE, in a 0.1 M KCl solution containing 5.0 mM $K_3[Fe(CN)_6]^{3-/4-}$; scan rate: 50 mV s^{-1}.

obtained plots and the results in the Table 1 reveal that the unmodified carbon paste (CPE) electrode had a very weak pseudo-reversible behavior with a ΔE_p value of 0.23 v; however, for the modified electrode with MOF and MWCNTs, the response improved and ΔE_p decreased. Finally, for the modified electrode with an optimal combination of Cr-MOF-MWCNT/CPE, the value of ΔE_p decreased to 0.12 V, which shows the reversible behavior of that modified electrode. In addition to these results, the intensity of the current of the oxidation and reduction peaks for the modified electrodes increased compared to that of the unmodified electrode. A comparison among the modified electrodes revealed that the current intensity of the oxidation and reduction peaks was higher for the carbon paste electrode modified with Cr-MOF-MWCNT, and this indicated the greater sensitivity of this electrode. Therefore, from the obtained results, the most sensitive electrode was the modified carbon paste electrode with a mixture of MOFs and MWCNTs. In order to investigate the characteristics of the modified electrodes compared to the unmodified electrodes in terms of their resistance and conductivity, electrochemical impedance spectroscopy (EIS) was performed. The Nyquist diagrams of the unmodified electrode (CPE) and the modified electrodes, including Cr-MOF/CPE, MWCNTs/CPE and the modified electrode with the optimal combination of MIL-101(Cr) and MWCNTs are presented in Fig. 4(b). The results obtained from these graphs are presented in Table 1. The R_{ct} related to the modified electrode (Cr-MOF-MWCNTs/CPE) had the lowest value compared to that of the other electrodes, which was due to the synergistic effect of the high surface absorption resulting from the MOF structure along with the high electrical conductivity of MWCNTs.

3.1.5. Electrochemical detection of CGA. In order to evaluate the sensitivity of the modified electrodes, cyclic voltammetry was used to measure a 0.5 mM CGA solution in a 0.1 M PB solution at pH 7.0. The cyclic voltammetry diagrams of the measured CGA was obtained from four electrodes, namely the CPE electrode, Cr-MOF/CPE electrode, MWCNTs/CPE electrode and Cr-MOF-MWCNTs/CPE electrode, are shown in Fig. 5. Analysis of the voltammogram indicates that CGA exhibits reversible electrochemical behavior, involving both oxidation and reduction processes. Compared to the blank CPE, the electrode modified with MWCNTs exhibits higher current intensity (due to higher electrical conductivity) at both anodic and cathodic peaks, making it more sensitive for the measurement of chlorogenic acid. On the other hand, a further reduction in the difference between the two potential peaks (ΔE_p) was observed due to the effect of the higher surface adsorption associated with the MOF modifier. The decreased current observed in the cyclic voltammogram can be due to the following reaction:

Table 1 CV responses and EIS data obtained from the iron tracer solution in contact with the surfaces of the unmodified and modified carbon paste electrodes

Electrode	$I_{p.a}$ (μA)	(μA) $I_{p.c}$	$E_{p.a}$ (V)	$E_{p.c}$ (V)	ΔE_p	R_{ct} (Ω)	R_s (Ω)
CPE	19/131	−19/138	0/29	0/06	0/23	9781.338	33.162
Cr-MOF/CPE	30/051	−31/574	0/25	0/09	0/16	5311.334	49.866
MWCNTs/CPE	39/592	−39/968	0/28	0/07	0/21	1708.629	72.771
Cr-MOF-MWCNTs/CPE	49/454	−48/281	0/23	0/11	0/12	348.42	136.82

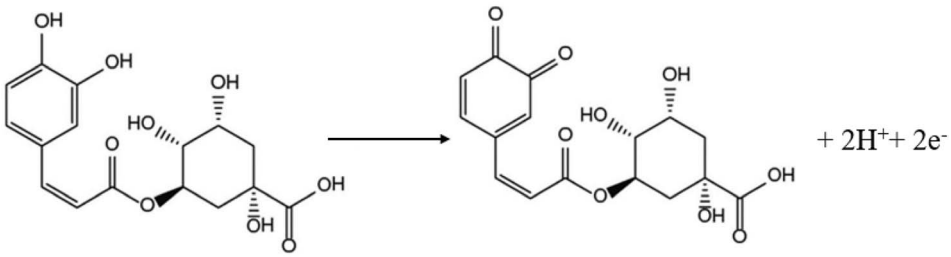

(1)

The cathodic and anodic peak currents of the CPE electrode were equal to 1.094 and −0.393 V, respectively, which increased to 3.377 and −2.005 for the Cr-MOF-MWCNTs/CPE electrode. The higher CGA current observed at a lower potential with the Cr-MOF-MWCNTs/CPE electrode was due to the high absorption properties of the Cr-MOF structure. Additionally, electrical conductivity increased due to the presence of MWCNTs in the electrode, which was due to an increase in the ability of the electrode to transfer charge.

3.1.6. Effect of pH on the oxidation and reduction of CGA. Fig. 6(a) shows the cyclic voltammograms of a 300 μM CGA solution with the modified electrode (Cr-MOF-MWCNTs/CPE) in the pH range of 3 to 8. The oxidation and reduction potentials of CGA shifted to a more negative potential as the pH increased from 3 to 8. In alkaline environments (higher pH), due to the reduced proton concentration, CGA oxidation was easily achieved and was not prevented. In an acidic environment, according to eqn (1) during the oxidation of CGA, hydroquinone is converted to quinone through the transfer of two electrons and two protons. Conversely, under alkaline conditions, the electrochemical reaction of CGA occurred without the involvement of proton transfer, with only two electrons being reduced. The plots of the peak oxidation current and potential of CGA against pH are shown in Fig. 6(b and c),

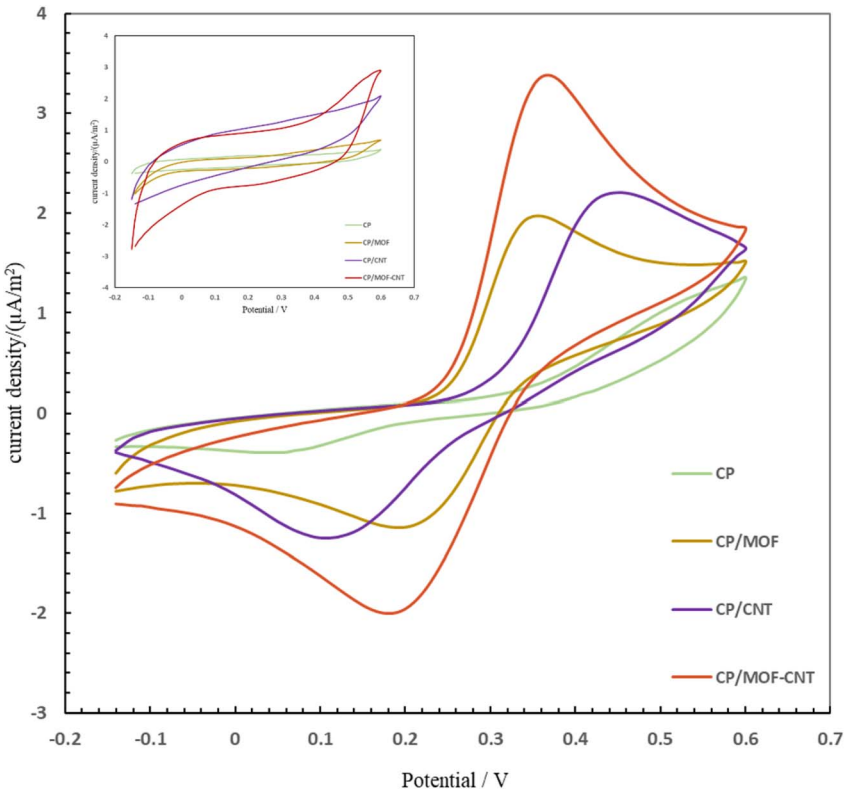

Fig. 5 Cyclic voltammograms of different modified electrodes, namely, CPE, MWCNTs/CPE, Cr-MOF/CPE, and Cr-MOF-MWCNTs/CPE, placed in 0.5 mM CGA in 0.1 M PB solution (pH = 7.0). Inset: cyclic voltammograms of different modified electrodes in a 0.1 M PB solution (pH 7.0); scan rate: 50 mV s^{-1}.

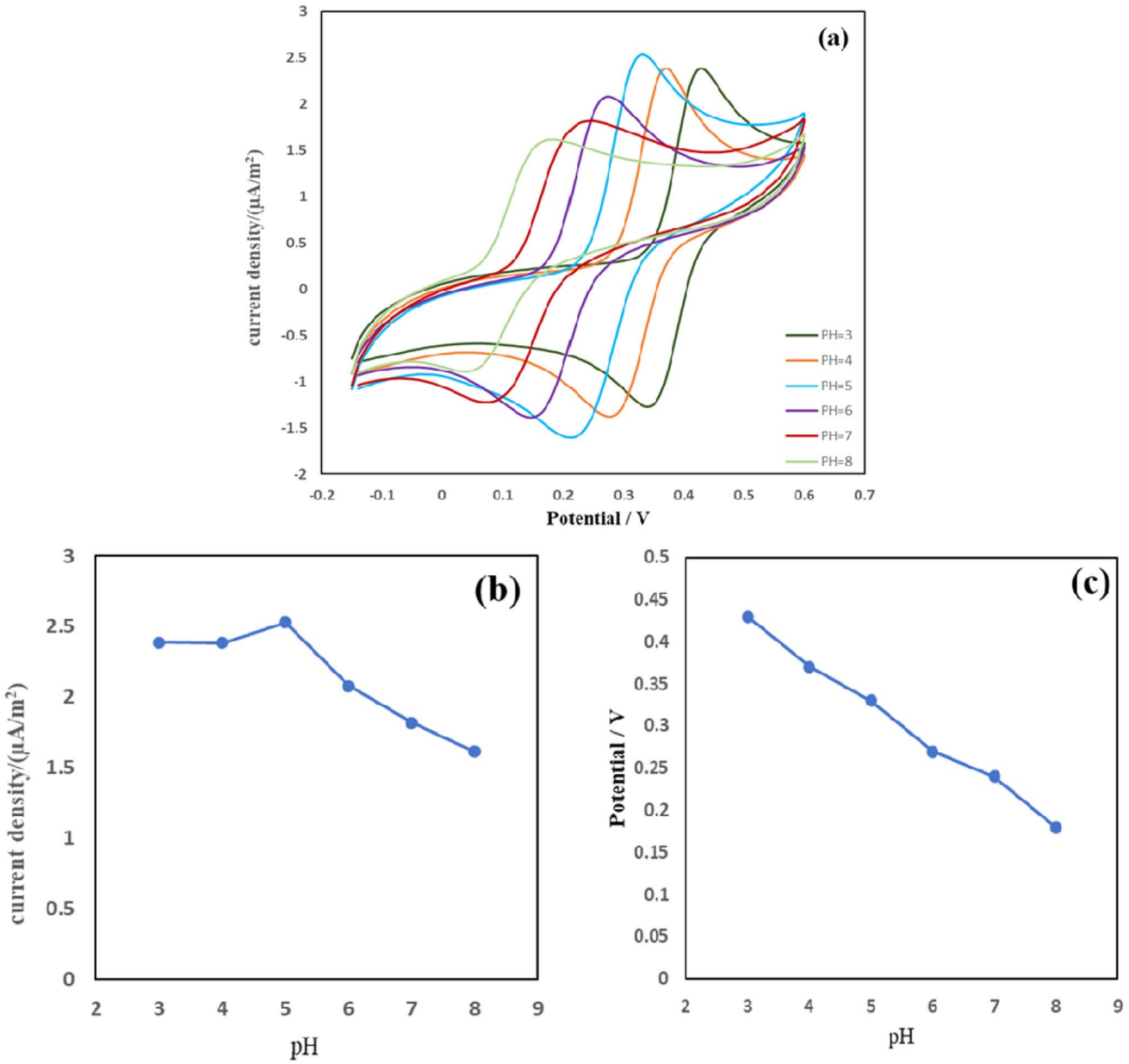

Fig. 6 Cyclic voltammograms of 300 μM CGA in a 0.1 M PB solution with Cr-MOF-MWCNTs/CPE (a) from pH = 3 to 8 and scan rate = 30 mV s^{-1}. (b) Plots of current density *vs.* pH and (c) potential *vs.* pH.

respectively. According to the Nernst equation, the relationship between peak potential (E_p) and pH for the oxidation of CGA is described as follows:

$$E_{pa} = -0.0486\ \text{pH} + 0.5705 \quad (2)$$

By applying the Nernst equation and analyzing the slope of the E_{pa} – pH graph, it was ascertained that two protons were exchanged. Moreover, the linear relationship ($R^2 = 0.994$) derived from this graph indicated that the number of electrons and protons involved in the oxidation of CGA was equal. Thus, the oxidation of CGA involved the transfer of two electrons and two protons. The current intensity of the anodic and cathodic peaks exhibited a gradual decrease as the pH increased from 3 to 8; however, a significant deviation occurred at pH 5, where the current reached its maximum. Consequently, pH 5 was selected as the optimal pH for CGA measurement in further experiments in this study.

3.1.7 Effect of scan rate on the oxidation and reduction of CGA. In order to understand the mechanism of the Cr-MOF-MWCNTs/CPE electrode, CV curves were plotted at different potential scan rates (Fig. 7(a)). In Fig. 7(b), a linear relationship was obtained by plotting the calibration curves derived from the currents of the cathodic and anodic peaks against $\upsilon^{1/2}$. The evaluation of the slope, which correlates the oxidation current of CGA with the square root of the scan rate, is indicated in eqn (3) and was derived from the Randles–Ševčik equation. This

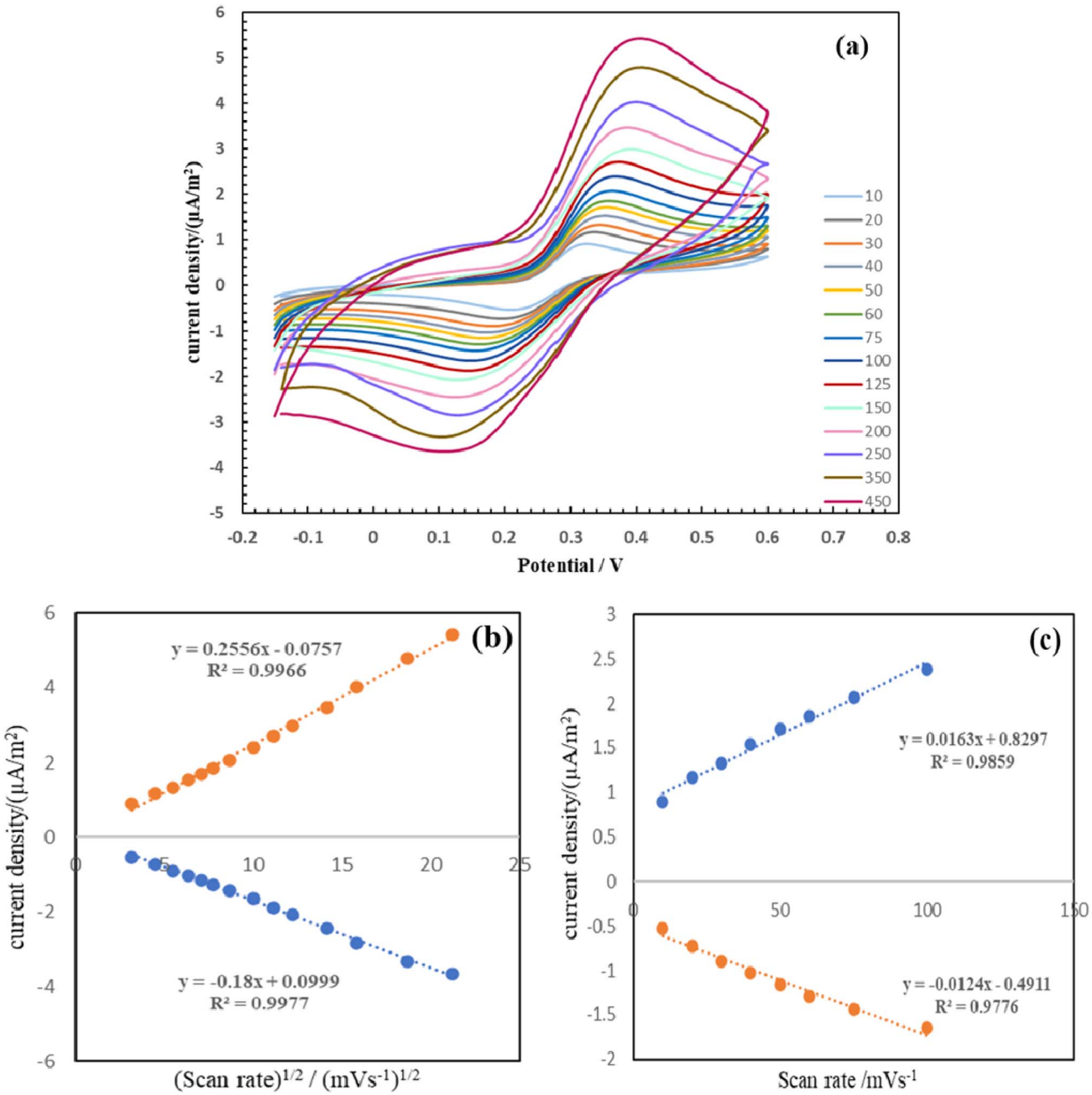

Fig. 7 Cyclic voltammograms of Cr-MOF-MWCNTs/CPE in 300 μM CGA at (a) different scan rates. Plots of (b) current density *vs.* scan rate$^{1/2}$ and (c) current density *vs.* scan rate.

evaluation suggests that the oxidation of CGA at the surface of the modified electrode was primarily influenced by mass transport phenomena. This finding further indicates that CGA must have first migrated to the electrode surface before participating in the oxidation reaction.

$$I_{pa} = 0.2556\, \upsilon^{1/2} - 0.0757 \quad (3)$$

The calibration curves based on the intensity of the oxidation and reduction currents of CGA *vs.* the scan rate (Fig. 7(c)) show a linear relationship between the cathodic and anodic peaks as a function of the potential scan rate, which means that there was a uniform distribution of the modifier on the electrode. The slope of this graph is linear at a low potential scan rate, indicating the absorption mechanism at the electrode.

Since the slope of both calibration graphs at low scan rate is related to the absorption mechanism, and the slope of the calibration graph at high scan rate is related to the penetration mechanism, both slopes were linear. Therefore, it can be concluded that the functional mechanism of the sensor involves both penetration and absorption, but the penetration

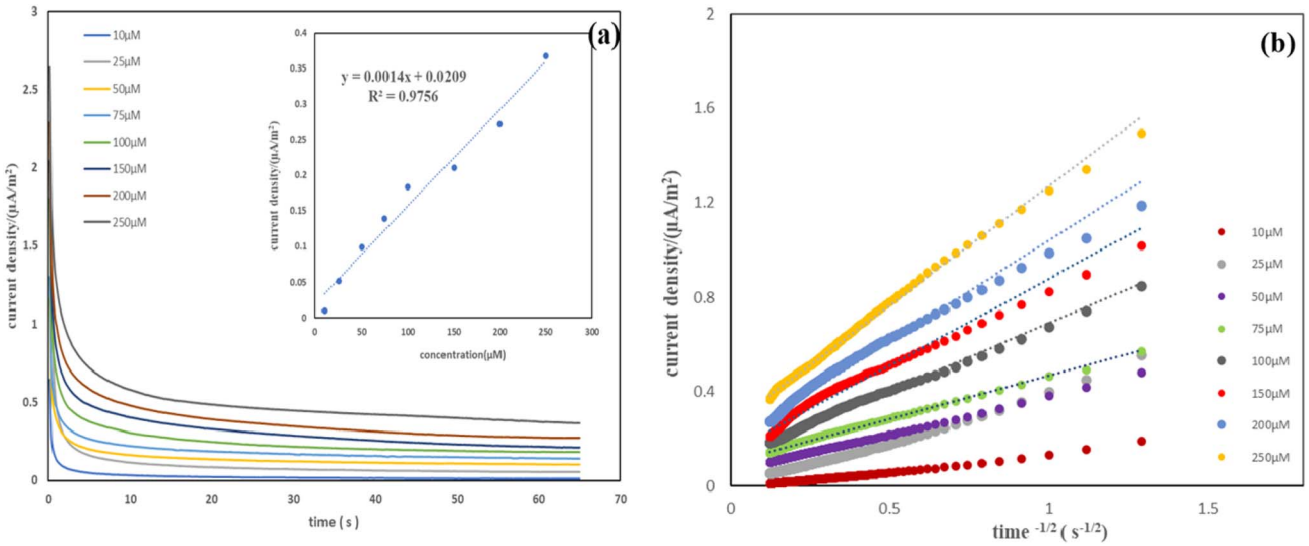

Fig. 8 (a) Chronoamperograms of the Cr-MOF-MWCNTs/CPE electrode in the presence of different concentrations of CGA in a 0.1 M PB solution recorded at 0.33 V. Inset: calibration curves of data. (b) Plots of current density *vs.* $t^{-1/2}$ based on the data from chronoamperograms in (a).

mechanism is more dominant because the slope of the current diagram based on $\upsilon^{1/2}$ is more linear.

3.1.8. Oxidation of CGA during chronoamperometry. Chronoamperometric testing was conducted for examining the electrochemical behavior of CGA during its reaction and determining its diffusion coefficient (D) at a potential of 0.33 V. These experiments utilized a Cr-MOF-MWCNTs/CPE electrode and spanned CGA concentrations ranging from 10 to 250 μM (Fig. 8(a)). A linear relationship with a coefficient of determination of $R^2 = 0.9756$ was observed for the current *versus* various concentrations of CGA at a specific time. This result indicates the sensitivity of the modified electrode for CGA detection. Furthermore, by plotting the intensity of the current for different CGA concentrations against the inverse of the square root of time ($t^{-1/2}$) as shown in Fig. 8(b), the slope of each plot was found to be proportional to $n\mathrm{FAD}^{1/2}\mathrm{C}\pi^{-1/2}$ based on Cottrell's equation. To eliminate the concentration variable from Cottrell's equation, a new line was plotted using the slopes obtained from Fig. 8(b) against the CGA concentrations, resulting in another linear relationship with a coefficient of determination of $R^2 = 0.9913$, and a slope corresponding to $n\mathrm{FAD}^{1/2}\pi^{-1/2}$. The active surface area of the electrode (A) was determined by applying the Randles–Ševčík equation, and the obtained number was equal to 6.03×10^{-3} cm^2. Finally, by substituting these parameters into Cottrell's equation, the diffusion coefficient (D) was determined to be 3.8×10^{-9} $\mathrm{cm}^2\ \mathrm{s}^{-1}$.

3.1.9. Oxidation of CGA and calculation of detection limit by DPV. To determine the sensitivity of the modified electrode Cr-MOF-MWCNTs/CPE, the voltammetric responses from DPV

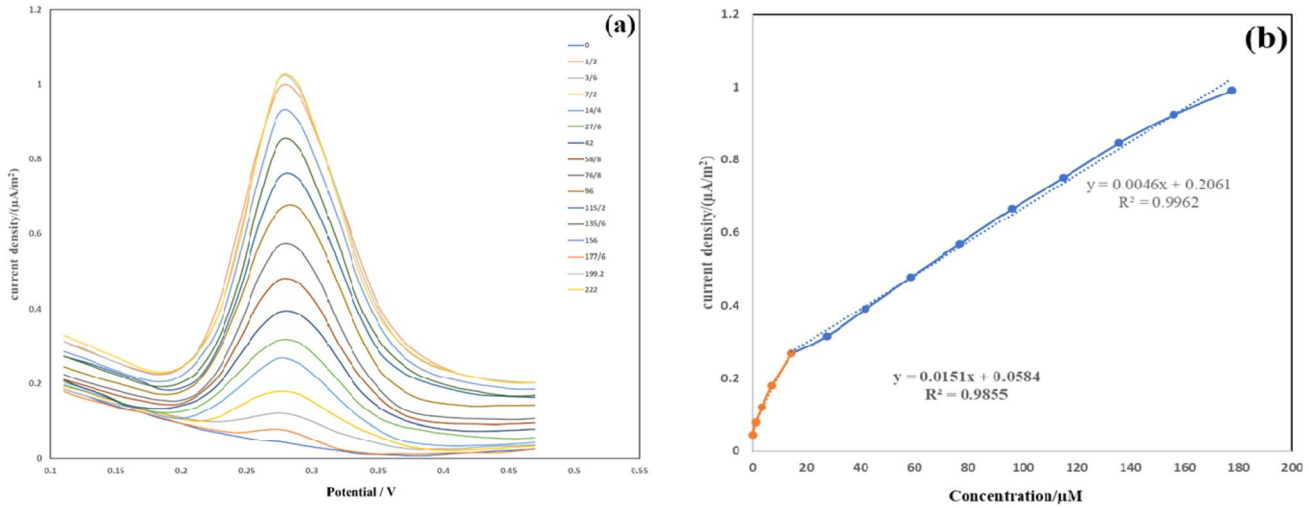

Fig. 9 (a) DPV curves of the Cr-MOF-MWCNTs/CPE electrode in the presence of different concentrations of CGA in a 0.1 M PB solution (pH 5.0) with a potential scan rate of 50 mV s^{-1}, and (b) calibration curves based on the obtained current density *vs.* CGA concentration.

were investigated after the successive injection of different concentrations of CGA into a 1.0 M phosphate buffer solution (pH 5) under continuous stirring at a potential scan rate of 50 mV s^{-1}. According to Fig. 9(a), after each addition of CGA, the intensity of the current measured by the modified electrode increased. By plotting the alterations in current against the CGA concentration, two linear regions with different slopes were obtained, as shown in Fig. 9(b).

The first linear range is for concentrations ranging from 0 to 14.4 μM, and its equation is expressed as:

$$I_{pa} = 0.0151\ C + 0.0584\ R^2 = 0.9855 \quad (4)$$

The second linear range is for concentrations ranging from 14.4 to 177.6 μM, and its equation is expressed as:

$$I_{pa} = 0.0046\ C + 0.2061\ R^2 = 0.9962 \quad (5)$$

The RSD of the CGA current during its oxidation potential in the buffer solution was calculated to establish the limit of detection (LOD). According to the calibration curve and the detection limit formula (LOD = 3 S_b/m), S_b, which is the slope of the calibration curve from the buffer solution, was equal to 0.001, the calibration curve for CGA exhibited a slope of 0.0151, and the LOD was calculated to be 0.0198 μM. The results

Table 2 Comparison of the detection limit and linear range of different electrodes for measuring CGA with those of the modified electrode developed in this work

Working electrode	Method	Linear range (μM)	LOD (μM)	Ref.
CuTCPP/pOMC-3/GCE	DPV	0.1–15	1.0	59
Ag–ZrO_2/GO/GCE	DPV	0.5–347	0.02	19
Fe_3O_4-MIL-100(Fe)/GCE	DPV	0.1–460	0.4	60
PASA/GCE	CV	0.4–12	0.0083	61
Ir-BMI·PF6-PPOx	SWV	3.48–49.50	0.0006	62
MOF-818@RGO/MWCNT-3/GCE	DPV	0.1–20	2	18
BDD electrode	SWV	5.64–147	0.0825	63
(MIL-101(Cr)/MWCNT/CPE)	DPV	0–177.6	0.01	This study

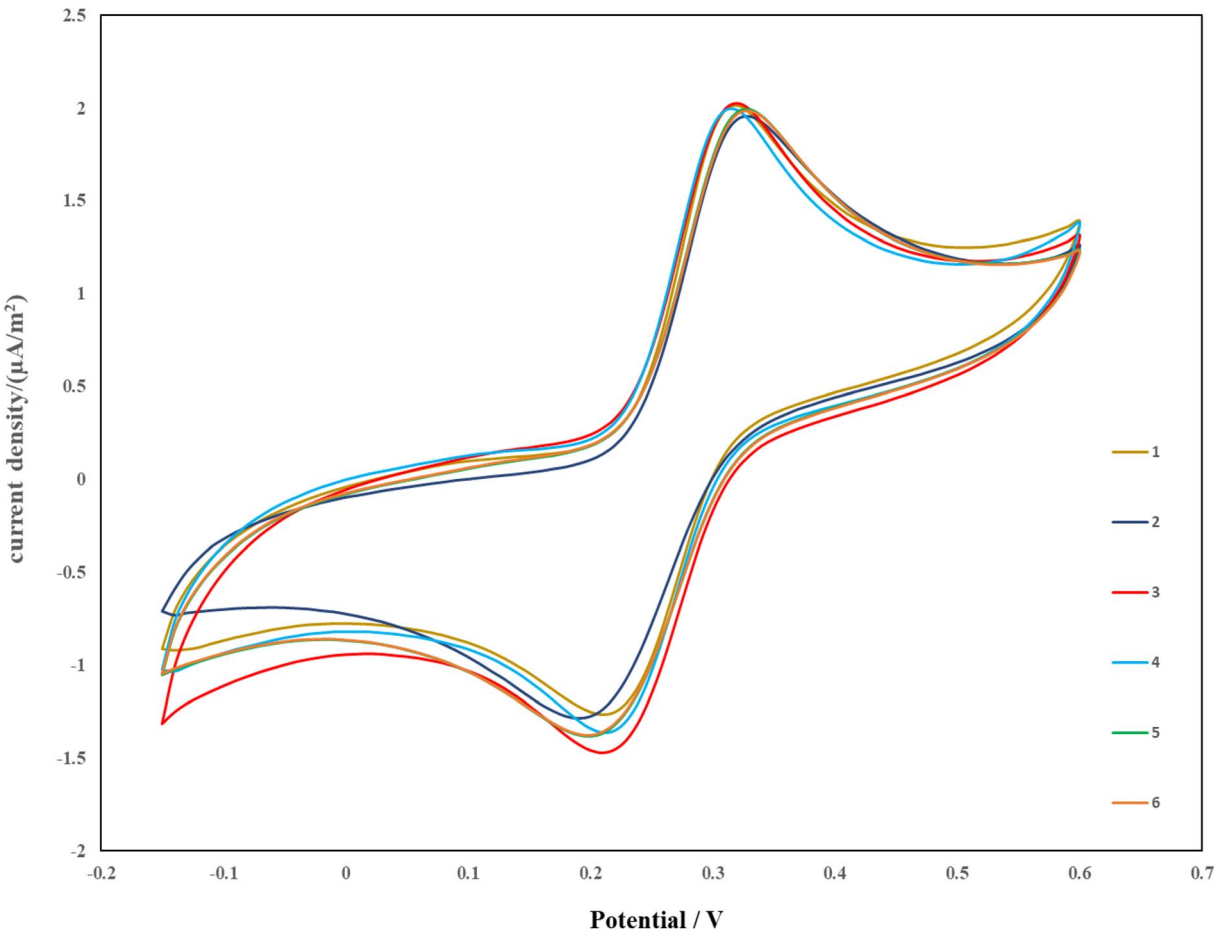

Fig. 10 Cyclic voltammograms obtained from the oxidation of CGA for evaluating the reproducibility of Cr-MOF-MWCNTs/CPE.

obtained from this study are shown in Table 2, which compares the results of similar reports for measuring CGA by electrochemical methods. This comparison shows that the sensor designed in this study is competitive with other sensors.

3.1.10. Reproducibility studies of Cr-MOF-MWCNTs/CPE. To study the reproducibility of the modified electrode (Cr-MOF-MWCNTs/CPE), three electrodes were fabricated under controlled and identical conditions (Fig. 10). Subsequently, each electrode underwent cyclic voltammetry in a 600 μM CGA solution. The relative standard deviation (RSD) of the obtained responses was calculated to be 1.25%, indicating a high reproducibility. For further assessment of the electrode's analytical performance for CGA detection, a 300 μM CGA solution was prepared in a buffer solution at pH 5.0. The modified electrode underwent six consecutive cyclic voltammetric scans, resulting in a RSD of 1.39% based on the measured current responses.

3.1.11. Stability results. To evaluate the long-term electrochemical stability of the CPE/MIL-101(Cr)-MWCNTs modified electrode, CV measurements were conducted in a 500 μM CGA solution prepared in a 0.1 M phosphate buffer (pH 5.0) (Fig. 11). The electrode was stored under ambient laboratory conditions and tested at three-day intervals, resulting in seven measurement points (days 1, 4, 7, 10, 13, 16, and 19). At each time point, the electrochemical response was recorded, and the peak oxidation current of CGA was monitored. The results demonstrated consistent peak current values with negligible fluctuations throughout the testing period. The calculated relative standard deviation (RSD) was 2.99%, indicating excellent long-term stability and reproducibility of the modified electrode. These findings underscore the electrode's reliability and suitability for sensor development and real-world analytical applications.

3.1.12. Measurement of CGA in real samples. The sensing ability of the fabricated electrode (Cr-MOF-MWCNTs/CPE) was studied by assessing the concentration of CGA in actual coffee samples, which included four types of green coffee beans. To extract CGA from each sample, the coffee beans were first ground and sieved, then 10.0 mg of each coffee powder was dissolved in 25.0 ml of distilled water, stirred for 30 minutes and slowly heated to 60 °C to dissolve the caffeine in water. Each solution was then filtered, and the remaining solid was placed in an ultrasonic bath with ethanol at 60 °C for 30 min to dissolve the CGA in the beans in the ethanol. At the end of this step, each ethanol solution containing CGA was filtered with the aid of a centrifuge, which was used for separating the suspended particles in the solution. The concentration of CGA in each coffee sample was measured by UV-vis spectrometry. Based on the spectrum of CGA obtained in previous literature methods, the absorbance of the samples was measured at $\lambda_{max} = 329$; 0.5 mL of a CGA standard solution was added for the measurements. For determining the concentration of the coffee samples, the intensity of the absorption is measured again at $\lambda_{max} = 329$. Using these measurements and eqn (6), the

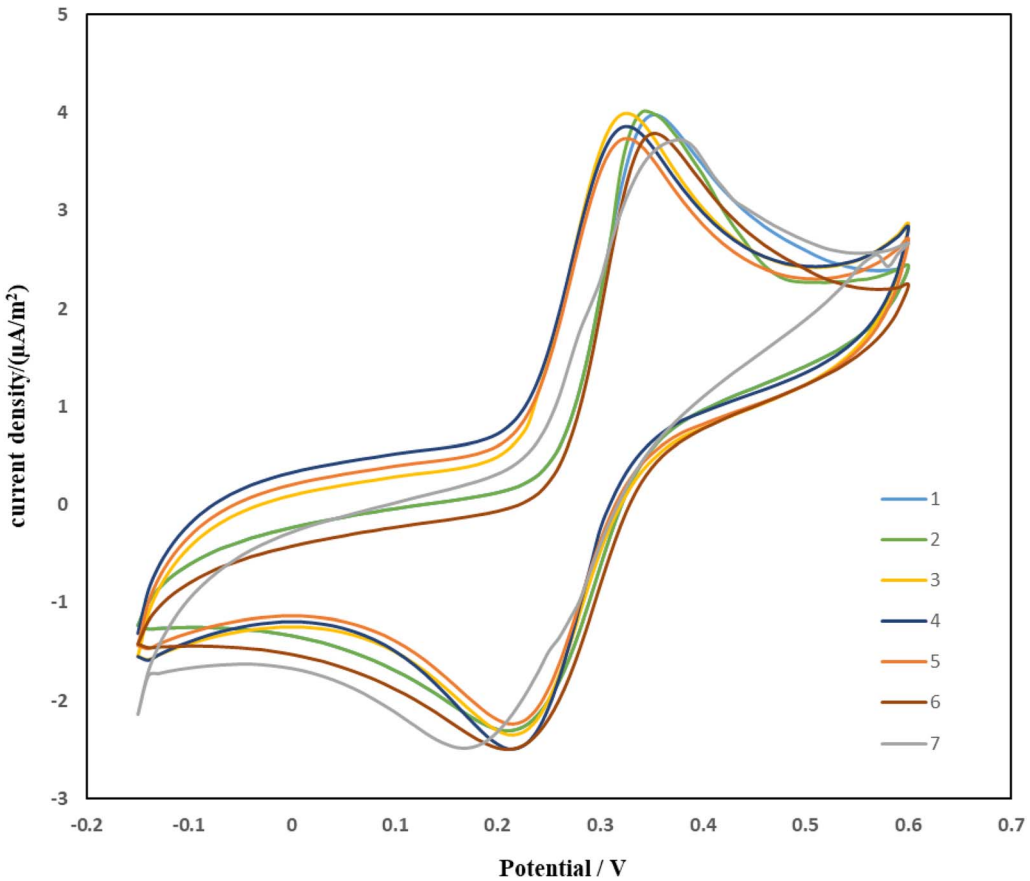

Fig. 11 Cyclic voltammograms of the Cr-MOF-MWCNTs/CPE electrode in a CGA solution for evaluating its long-term electrochemical stability.

Table 3 Calculation of the CGA concentration in different coffee samples by UV-vis spectroscopy and electrochemical method

	UV-vis spectroscopy			Electrochemical method			
Sample	Absorption (before adding the standard)	Absorption (after adding the standard)	Concentration	Current intensity (before adding the standard)	Current intensity (after adding the standard)	Concentration	Error percentage
1	3.8315	3.9541	299.1	0.9339	0.9651	293.8	1.7%
2	3.5908	3.7179	286.8	0.7811	0.8105	279.3	2.6%
3	3.3701	3.4935	282.7	0.6702	0.6957	277.9	1.7%
4	3.7711	3.8937	297.1	0.8363	0.8643	293.6	1.2%

concentration of CGA in the coffee samples was obtained.[64] In order to check the capability of our fabricated electrode, a differential pulse voltammetry technique was used. In this technique, 0.1 ml of each prepared coffee sample was dissolved in 10 ml of phosphate buffer with a pH of 0.5. The flow intensity was obtained from the DPV diagram, and then, 0.5 mL of a CGA standard sample was added to each coffee sample and the flow intensity was measured. Finally, with the help of eqn (6), the concentration of CGA in the coffee samples was obtained.

$$C_u = A_1 C_s V_s / A_2 V_t - A_1 V_u \quad (6)$$

Based on the findings presented in Table 3, the concentrations of CGA detected in the coffee beans demonstrate a strong correlation with the actual values. A comparison of the percentage differences between the electrochemical method used in this study and the UV-vis method underscores the effectiveness of the developed sensor. These results indicate that the concentrations obtained through this electrochemical approach are both accurate and reliable.

4. Conclusions

In this work, a sensitive, simple and cost-effective method was developed to measure CGA using a carbon paste electrode modified with Cr-MOF-MWCNT. This electrode exhibited a strong response to the oxidation and reduction of CGA. Resulting in an approximately threefold increase in the current intensity of the corresponding peaks. Additionally, the LOD of this sensor, determined using differential pulse voltammetry, was 0.0198 μM, which is very close and comparable to the detection limit of electrodes designed in previous studies (Table 2). The repeatability of this method has a relative standard deviation of 1.39% and a reproducibility with a relative standard deviation of 1.25%. In order to evaluate and measure the modified electrode's capability for determining the amount of CGA present in real samples, such as green coffee beans, concentration values obtained from the standard UV-vis method were compared with concentration values obtained from the electrochemical method. From the comparison, the percentage relative error obtained was on average between 1% and 4%. Therefore, we were able to design a sensitive and reliable sensor for CGA measurement in this study.

Conflicts of interest

The authors declare that there are no conflicts of interest.

Data availability

The authors confirm that the data supporting the findings of this study are available within the article. Additional data are available from the corresponding author upon reasonable request.

Acknowledgements

The authors are grateful to the council of Qom University and University of Kashan for supporting this work by Grant No. (159271/MKK8) and to Samia Jafari, PhD in Analytical Chemistry, for advice regarding the work.

References

1 M. Naveed, V. Hejazi, M. Abbas, A. A. Kamboh, G. J. Khan, M. Shumzaid, *et al.*, Chlorogenic acid (CGA): A pharmacological review and call for further research, *Biomed. Pharmacother.*, 2018, **97**, 67–74.

2 S. Meng, J. Cao, Q. Feng, J. Peng and Y. Hu, Roles of chlorogenic acid on regulating glucose and lipids metabolism: a review. Evidence-based complementary and alternative medicine, *Evid. base Compl. Alternative Med.*, 2013, **2013**, 801457.

3 I. Tomac and M. Šeruga, Electrochemical properties of chlorogenic acids and determination of their content in coffee using differential pulse voltammetry, *Int. J. Electrochem. Sci.*, 2016, **11**(4), 2854.

4 I.-G. Munteanu and C. Apetrei, Electrochemical determination of chlorogenic acid in nutraceuticals using voltammetric sensors based on screen-printed carbon electrode modified with graphene and gold nanoparticles, *Int. J. Mol. Sci.*, 2021, **22**(16), 8897.

5 V. Mariyappan, S.-M. Chen, T. Jeyapragasam and J. M. Devi, Designing and construction of a cobalt-metal-organic framework/heteroatoms co-doped reduced graphene oxide mesoporous nanocomposite based efficient electrocatalyst for chlorogenic acid detection, *J. Alloys Compd.*, 2022, **898**, 163028.

6 N. Alpar, Y. Yardım and Z. Şentürk, Selective and simultaneous determination of total chlorogenic acids, vanillin and caffeine in foods and beverages by adsorptive stripping voltammetry using a cathodically pretreated boron-doped diamond electrode, *Sens. Actuators, B*, 2018, **257**, 398–408.

7 Y. Hao, R. Gao, D. Liu, G. He, Y. Tang and Z. Guo, Selective extraction and determination of chlorogenic acid in fruit juices using hydrophilic magnetic imprinted nanoparticles, *Food Chem.*, 2016, **200**, 215–222.

8 J. Santana-Gálvez, L. Cisneros-Zevallos and D. A. Jacobo-Velázquez, Chlorogenic acid: Recent advances on its dual role as a food additive and a nutraceutical against metabolic syndrome, *Molecules*, 2017, **22**(3), 358.

9 W. Xu, X. Zhang, L. Wang, W. Zeng, Y. Sun, C. Zhou, *et al.*, Effect of chlorogenic acid on the quorum-sensing system of clinically isolated multidrug-resistant Pseudomonas aeruginosa, *J. Appl. Microbiol.*, 2022, **132**(2), 1008–1017.

10 Y. Mei, H. Sun, G. Du, X. Wang and D. Lyu, Exogenous chlorogenic acid alleviates oxidative stress in apple leaves by enhancing antioxidant capacity, *Sci. Hortic.*, 2020, **274**, 109676.

11 H. Lu, Z. Tian, Y. Cui, Z. Liu and X. Ma, Chlorogenic acid: A comprehensive review of the dietary sources, processing effects, bioavailability, beneficial properties, mechanisms of action, and future directions, *Compr. Rev. Food Sci. Food Saf.*, 2020, **19**(6), 3130–3158.

12 Y. Yang, P. Wang, Z. Luo, J. Li, Y. Wang, Z. Li, *et al.*, Enhanced electrocatalytic activity of 2D ordered mesoporous nitrogen-rich carbon nanosheets functional NiFe2O4 nanospheres for ultrasensitive detection of chlorogenic acid in natural samples, *Chem. Eng. J.*, 2023, 143815.

13 T. Pal, S. Mohiyuddin and G. Packirisamy, Correction to "Facile and Green Synthesis of Multicolor Fluorescence Carbon Dots from Curcumin: *In Vitro* and *in Vivo* Bioimaging and Other Applications", *ACS Omega*, 2018, **3**(5), 5887.

14 R. Chokkareddy, G. G. Redhi and T. Karthick, A lignin polymer nanocomposite based electrochemical sensor for the sensitive detection of chlorogenic acid in coffee samples, *Heliyon*, 2019, **5**(3), e01457.

15 X. Hu, L. Wang, Y. He, M. Wei, H. Yan and H. Zhu, Chlorogenic acid promotes osteogenic differentiation of human dental pulp stem cells through Wnt signaling, *Stem Cells Dev.*, 2021, **30**(12), 641–650.

16 B. K. Bassoli, P. Cassolla, G. R. Borba-Murad, J. Constantin, C. L. Salgueiro-Pagadigorria, R. B. Bazotte, *et al.*, Chlorogenic acid reduces the plasma glucose peak in the oral glucose tolerance test: effects on hepatic glucose release and glycaemia, *Cell Biochem. Funct.*, 2008, **26**(3), 320–328.

17 K. Fujioka and T. Shibamoto, Chlorogenic acid and caffeine contents in various commercial brewed coffees, *Food Chem.*, 2008, **106**(1), 217–221.

18 Y. Yan, X. Bo and L. Guo, MOF-818 metal-organic framework-reduced graphene oxide/multiwalled carbon nanotubes composite for electrochemical sensitive detection of phenolic acids, *Talanta*, 2020, **218**, 121123.

19 K. Alagumalai, R. Shanmugam, S.-M. Chen, B. Arumugam, T.-W. Chen, J. Yu, *et al.*, A portable advanced electrocatalyst for polyphenolic chlorogenic acid evaluation in food samples, *Chem. Eng. J.*, 2022, **435**, 134796.

20 W. Cheng, J. Huang, C. Liu, Q. Zeng, Y. Tong, L. Wang, *et al.*, High sensitivity chlorogenic acid detection based on multiple layer-by-layer self-assembly films of chitosan and multi-walled carbon nanotubes on a glassy carbon electrode, *RSC Adv.*, 2017, **7**(12), 6950–6956.

21 M. Amin, S. Sharif, S. Akram, G. Muhammad, S. Amin, R. Ashraf, *et al.*, A dispersive liquid–liquid microextraction followed by reverse-phase high-performance liquid chromatography for QuEChERS determination of chlorogenic acid, *Phytochem. Anal.*, 2023, **34**(1), 30–39.

22 Z. Zhou, S. Liang, X. Zou, Y. Teng, W. Wang and L. Fu, Determination of Phenolic Acids Using Ultra-High-Performance Liquid Chromatography Coupled with Triple Quadrupole (UHPLC-QqQ) in Fruiting Bodies of Sanghuangporus baumii (Pilát) LW Zhou and YC Dai, *Plants*, 2023, **12**(20), 3565.

23 W. Xie, Y. Yu, M. Hou, Y. Zhang, H. Yu, H. Zhang, *et al.*, Simultaneous separation and determination of five

chlorogenic acid isomers in Honeysuckle by capillary electrophoresis using self-synthesized ionic liquid [N-methylimidazole-β-cyclodextrin][bromide] as separation selector, *J. Sep. Sci.*, 2022, **45**(16), 3197–3207.

24 P. Tong, L. Zhang, Y. He, Y. Chi and G. Chen, A simple capillary electrophoresis with electrochemical detection method for determination of the hydrolysis rate constant of chlorogenic acid, *Talanta*, 2009, **77**(5), 1790–1794.

25 J. Zhu, S. Qi, J. Li and X. Chen, Low-temperature bath/high-conductivity zone/stacking micellar electrokinetic chromatography for the analysis of phenolic acids in coffee drink, *J. Chromatogr. A*, 2008, **1212**(1–2), 137–144.

26 J. Zhang, M. Chen, W. Ju, S. Liu, M. Xu, J. Chu, *et al.*, Liquid chromatograph/tandem mass spectrometry assay for the simultaneous determination of chlorogenic acid and cinnamic acid in plasma and its application to a pharmacokinetic study, *J. Pharm. Biomed. Anal.*, 2010, **51**(3), 685–690.

27 Z. Xia, Y. Sun, C. Cai, Y. He and P. Nie, Rapid determination of chlorogenic acid, luteoloside and 3, 5-o-dicaffeoylquinic acid in chrysanthemum using near-infrared spectroscopy, *Sensors*, 2019, **19**(9), 1981.

28 B.-C. Gu, K.-J. Chung, B.-W. Chen, Y.-H. Dai and C.-C. Wu, Electrochemical detection combined with artificial neural networks for the simultaneous intelligent sensing of caffeine and chlorogenic acid, *Electrochim. Acta*, 2023, **463**, 142820.

29 T. Teker and M. Aslanoglu, A novel voltammetric sensing platform based on carbon nanotubes-niobium nanoparticles for the determination of chlorogenic acid, *Arabian J. Chem.*, 2020, **13**(5), 5517–5525.

30 I. M. Apetrei and C. Apetrei, Development of a novel biosensor based on tyrosinase/platinum nanoparticles/chitosan/graphene nanostructured layer with applicability in bioanalysis, *Materials*, 2019, **12**(7), 1009.

31 E. Beyyavaş and M. Aslanoglu, Construction of an electrochemical sensing platform for the sensitive determination of chlorogenic acid in locally consumed bitter coffee known as Mirra, *Food Chem.*, 2023, 136600.

32 T. Wan, Z. Zhang, H. Wang, Y. Yang, H. Yang, J. Zhang, *et al.*, Rapid and highly selective detection of chlorogenic acid in fruit samples by Fe 3 O 4@ SiO 2@ PIL with boron affinity *via* a fluorescence enhanced strategy, *New J. Chem.*, 2023, **47**(2), 828–837.

33 J. Ganesamurthi, R. Shanmugam, S.-M. Chen, K. Alagumalai, M. Balamurugan and Y.-Y. Yu, Binary transition metal oxide based electrochemical sensor for the evaluation of chlorogenic acid in real-time samples, *Mater. Chem. Phys.*, 2022, **292**, 126757.

34 A. J. J. Amalraj and S.-F. Wang, Influence of mineralizer in the preparation of Bi2CuO4 sensor for the electrochemical evaluation of chlorogenic acid in various real-time samples, *Mater. Today Chem.*, 2022, **26**, 101154.

35 M. Li, G. Zhang, A. Boakye, H. Chai, L. Qu and X. Zhang, Recent advances in metal-organic framework-based electrochemical biosensing applications, *Front. Bioeng. Biotechnol.*, 2021, **9**, 797067.

36 M. Linares-Moreau, L. A. Brandner, MdJ. Velásquez-Hernández, J. Fonseca, Y. Benseghir, J. M. Chin, *et al.*, Fabrication of Oriented Polycrystalline MOF Superstructures, *Adv. Mater.*, 2023, 2309645.

37 M. Moharramnejad, A. Ehsani, M. Shahi, S. Gharanli, H. Saremi, R. E. Malekshah, *et al.*, MOF as nanoscale drug delivery devices: Synthesis and recent progress in biomedical applications, *J. Drug Delivery Sci. Technol.*, 2023, 104285.

38 H. Daglar, H. C. Gulbalkan, G. Avci, G. O. Aksu, O. F. Altundal, C. Altintas, *et al.*, Effect of metal–organic framework (MOF) database selection on the assessment of gas storage and separation potentials of MOFs, *Angew. Chem., Int. Ed.*, 2021, **60**(14), 7828–7837.

39 X. Fang, B. Zong and S. Mao, Metal–organic framework-based sensors for environmental contaminant sensing, *Nano-Micro Lett.*, 2018, **10**, 1–19.

40 M. Moharramnejad, A. Ehsani, S. Salmani, M. Shahi, R. E. Malekshah, Z. S. Robatjazi, *et al.*, Zinc-based metal-organic frameworks: Synthesis and recent progress in biomedical application, *J. Inorg. Organomet. Polym. Mater.*, 2022, **32**(9), 3339–3354.

41 H. Cui, S. Cui, Q. Tian, S. Zhang, M. Wang, P. Zhang, *et al.*, Electrochemical sensor for the detection of 1-hydroxypyrene based on composites of PAMAM-regulated chromium-centered metal–organic framework nanoparticles and graphene oxide, *ACS Omega*, 2021, **6**(46), 31184–31195.

42 L. Liu, Y. Zhou, S. Liu and M. Xu, The applications of metal–organic frameworks in electrochemical sensors, *ChemElectroChem*, 2018, **5**(1), 6–19.

43 S. Jafari, S. M. Pourmortazavi, A. Ehsani and S. Mirsadeghi, Cobalt-based metal-organic framework-functionalized graphene oxide modified electrode as a new electrochemical sensing platform for detection of free chlorine in aqueous solution, *Anal. Biochem.*, 2023, **681**, 115334.

44 J. A. Cruz-Navarro, F. Hernandez-Garcia and G. A. A. Romero, Novel applications of metal-organic frameworks (MOFs) as redox-active materials for elaboration of carbon-based electrodes with electroanalytical uses, *Coord. Chem. Rev.*, 2020, **412**, 213263.

45 T. T. Tung, M. T. Tran, J.-F. Feller, M. Castro, T. Van Ngo, K. Hassan, *et al.*, Graphene and metal organic frameworks (MOFs) hybridization for tunable chemoresistive sensors for detection of volatile organic compounds (VOCs) biomarkers, *Carbon*, 2020, **159**, 333–344.

46 K. M. Qasem, S. Khan, S. Chinnam, H. A. Saleh, I. Mantasha, M. Zeeshan, *et al.*, Sustainable fabrication of Co-MOF@ CNT nano-composite for efficient adsorption and removal of organic dyes and selective sensing of Cr (VI) in aqueous phase, *Mater. Chem. Phys.*, 2022, **291**, 126748.

47 Y. Fu, J. Dai, Y. Ge, Y. Zhang, H. Ke and W. Zhang, A novel non-enzymatic electrochemical hydrogen peroxide sensor based on a metal-organic framework/carbon nanofiber composite, *Molecules*, 2018, **23**(10), 2552.

48 S. Iijima, Helical microtubules of graphitic carbon, *Nature*, 1991, **354**(6348), 56–58.

49 H. Meskher, T. Ragdi, A. K. Thakur, S. Ha, I. Khelfaoui, R. Sathyamurthy, *et al.*, A review on CNTs-based electrochemical sensors and biosensors: unique properties and potential applications, *Crit. Rev. Anal. Chem.*, 2023, 1–24.
50 M. N. Norizan, M. H. Moklis, S. Z. N. Demon, N. A. Halim, A. Samsuri, I. S. Mohamad, *et al.*, Carbon nanotubes: Functionalisation and their application in chemical sensors, *RSC Adv.*, 2020, **10**(71), 43704–43732.
51 F. Guo, T. Kang, Z. Liu, B. Tong, L. Guo, Y. Wang, *et al.*, Advanced lithium metal–carbon nanotube composite anode for high-performance lithium–oxygen batteries, *Nano Lett.*, 2019, **19**(9), 6377–6384.
52 C. B. Jacobs, M. J. Peairs and B. J. Venton, Carbon nanotube based electrochemical sensors for biomolecules, *Anal. Chim. Acta*, 2010, **662**(2), 105–127.
53 G. Huang, F. Zhang, X. Du, Y. Qin, D. Yin and L. Wang, Metal organic frameworks route to *in situ* insertion of multiwalled carbon nanotubes in Co3O4 polyhedra as anode materials for lithium-ion batteries, *ACS Nano*, 2015, **9**(2), 1592–1599.
54 N. A. Qasem, N. U. Qadir, R. Ben-Mansour and S. A. Said, Synthesis, characterization, and CO2 breakthrough adsorption of a novel MWCNT/MIL-101 (Cr) composite, *J. CO2 Util.*, 2017, **22**, 238–249.
55 H. M. Gobara, R. S. Mohamed, S. A. Hassan, F. H. Khalil and M. S. El-Sall, Pt and Ni nanoparticles anchored into metal–organic frameworks MIL-101 (Cr) as swift catalysts for ethanol dehydration, *Catal. Lett.*, 2016, **146**, 1875–1885.
56 Y. Zhou, Y. He, R. Wang, Y. Mao, J. Bai and Y. Dou, Modification of Multiwalled Carbon Nanotubes and Their Mechanism of Demanganization, *Molecules*, 2023, **28**(4), 1870.
57 J. Shadmehr, S. Zeinali and M. Tohidi, Synthesis of a chromium terephthalate metal organic framework and use as nanoporous adsorbent for removal of diazinon organophosphorus insecticide from aqueous media, *J. Dispersion Sci. Technol.*, 2019, **40**(10), 1–18.
58 E. Niknam, F. Panahi, F. Daneshgar, F. Bahrami and A. Khalafi-Nezhad, Metal–organic framework MIL-101 (Cr) as an efficient heterogeneous catalyst for clean synthesis of benzoazoles, *ACS Omega*, 2018, **3**(12), 17135–17144.
59 X. Zhao, T. Cui, R. Guo, Y. Liu, X. Wang, Y.-x An, *et al.*, A clean-up method for determination of multi-classes of persistent organic pollutants in sediment and biota samples with an aliquot sample, *Anal. Chim. Acta*, 2019, **1047**, 71–80.
60 Y. Chen, W. Huang, K. Chen, T. Zhang, Y. Wang and J. Wang, A novel electrochemical sensor based on core-shell-structured metal-organic frameworks: The outstanding analytical performance towards chlorogenic acid, *Talanta*, 2019, **196**, 85–91.
61 M. Chao and X. Ma, Voltammetric determination of chlorogenic acid in pharmaceutical products using poly (aminosulfonic acid) modified glassy carbon electrode, *J. Food Drug Anal.*, 2014, **22**(4), 512–519.
62 T. Teker, A. M. H. Hasan and M. Aslanoglu, A Boron Doped Diamond Electrode Modified with Nano-carbon Black for the Sensitive Electrochemical Determination of Chlorogenic Acid, *Electroanalysis*, 2019, **31**(12), 2446–2454.
63 Y. Yardım, E. Keskin and Z. Şentürk, Voltammetric determination of mixtures of caffeine and chlorogenic acid in beverage samples using a boron-doped diamond electrode, *Talanta*, 2013, **116**, 1010–1017.
64 A. Belay and A. Gholap, Characterization and determination of chlorogenic acids (CGA) in coffee beans by UV-Vis spectroscopy, *Afr. J. Pure Appl. Chem.*, 2009, **3**(11), 234–240.